

# Angular distributions of Ar reflected from molten metal surfaces

A. Muis and J. R. Manson

*Department of Physics and Astronomy, Clemson University, Clemson, South Carolina 29634*

(Received 11 December 1998; accepted 26 March 1999)

Recent experimental measurements of the angular distributions of monoenergetic beams of Ar atoms, with incident energies of up to 1 eV scattered from a molten In surface, are compared with calculated intensities. The data are described by classical scattering theory and the agreement indicates that the shapes of the lobes are dominated by single collisions with the surface, and the interaction potential has a smooth repulsive barrier similar to that commonly used to describe rare-gas scattering from crystalline metals. The attractive adsorption well of the interaction potential is considered, and is shown to have significant effects on the angular distributions at low incident energy. The dependence of the angular distributions on surface temperature is also well described.

© 1999 American Institute of Physics. [S0021-9606(99)70124-8]

## I. INTRODUCTION

Understanding the scattering distribution of a single atomic or molecular projectile incident on a clean surface is the problem fundamental to a description of the energy transfer and forces acting at a surface under conditions of rarefied gas flow. Clearly, the choice of a rare gas as the probing projectile provides the least complicated atom-surface interaction potential and, hence, can produce surface sensitive information with the simplest analysis.<sup>1,2</sup> For example, He atom scattering at thermal and hyperthermal energies has produced enormous amounts of detailed information on surface structure and dynamics for metals, semiconductors, and insulators.<sup>3</sup> However, He atoms at energies of up a hundred meV or more act as quantum-mechanical particles. On the other hand, the more massive rare gases at these same incident energies can often be treated with classical mechanics, yet the energy is still sufficiently low that the probability of excitation of atomic states or creation of surface damage is negligible.<sup>4</sup> Thus the heavier rare gases such as Ar are potentially a highly useful tool as a probe of surface structure and dynamics.

A series of new and very interesting experiments recently has been carried out for the scattering of the heavier rare gases Ne, Ar, and Xe from the molten metal surfaces of Ga, In, and Bi.<sup>5,6</sup> The energy-resolved scattering intensities<sup>5</sup> have been examined with classical scattering theory<sup>4</sup> and the comparison with data indicates that the scattering can be basically described as binary collisions with the substrate atoms with important contributions coming from multiple collisions with the surface. Further analysis of the temperature dependence of this energy-resolved data<sup>7</sup> indicated that these molten metal surfaces act as smooth but corrugated repulsive barriers similar to the types of potentials found for the case of He atom scattering from metal crystal surfaces.<sup>1,8</sup>

Recently, additional data have become available on the scattered total angular distributions for monoenergetic Ar beams incident on the liquid In surface at several different initial energies of up to one eV.<sup>5,6,9</sup> Initial analysis of this data using a molecular-dynamics simulation, in which the

scattering process and the In liquid were described by Lennard-Jones pairwise potential models, indicated that classical scattering theory is adequate to describe this system.<sup>9</sup> In this note it is suggested that these new data can be explained in the context of a relatively simple classical scattering theory, but that these experiments further narrow the possible scattering models, and hence, give a more precise picture of the interaction.

## II. THEORY

In the classical limit of large incident energies and high surface temperatures the scattering of an atomic projectile by a continuous, smooth, vibrating surface can be described by a differential reflection coefficient for scattering an incident beam of particles with momentum  $\mathbf{p}_i$  into the small final solid angle  $d\Omega_f$  and small final energy interval  $dE_f$ . The result is given by<sup>10-12</sup>

$$\frac{dR(\mathbf{p}_f, \mathbf{p}_i)}{d\Omega_f dE_f} = \frac{m^2 v_R^2 |\mathbf{p}_f|}{4\pi^3 \hbar^2 p_{iz} S_{u.c.}} |\tau_{fi}|^2 \left( \frac{\pi}{\Delta E_0 k_B T_S} \right)^{3/2} \times \exp \left\{ - \frac{(E_f - E_i + \Delta E_0)^2 + 2v_R^2 \mathbf{P}^2}{4k_B T_S \Delta E_0} \right\}, \quad (1)$$

where  $E_f$  and  $E_i$  are the final and initial energy of the projectile whose energy in a given momentum state  $\mathbf{p}_q$  is given by  $E_q = \mathbf{p}_q^2/2m$  with  $m$  the projectile mass.  $T_S$  is the surface temperature and  $k_B$  is the Boltzmann constant,  $S_{u.c.}$  is the area of a surface unit cell,  $v_R$  is a weighted average of phonon velocities at the surface,<sup>10</sup>  $|\tau_{fi}|^2$  is the scattering form factor,  $\hbar$  is the Planck constant, and  $\Delta E_0$  is the recoil energy. The momentum of a projectile is decomposed into components parallel and perpendicular to the surface according to  $\mathbf{p}_q = (\mathbf{P}_q, p_{qz})$  with the  $z$  axis taken as normal to the surface and  $\mathbf{P} = \mathbf{P}_f - \mathbf{P}_i$  is the parallel momentum transfer. The recoil energy appearing in Eq. (1) is, in the simplest case, given by  $\Delta E_0 = \mathbf{p}^2/2M$  where  $\mathbf{p} = \mathbf{p}_f - \mathbf{p}_i$  is the scattering vector and  $M$  is the mass of a surface atom. The Gaussian-like term in the

parallel momentum transfer  $\mathbf{P}$  in Eq. (1) arises from vibrational correlations of adjacent parts of the smooth repulsive surface due to vibrations polarized both parallel and perpendicular to the surface, and this is the only dependence of Eq. (1) on the actual form of the surface phonon spectral density. The parameter  $v_R$  appearing in this Gaussian-like term can be calculated from the phonon spectral density and for smooth, close-packed metal surfaces is expected to be of the order of the Rayleigh phonon velocity.<sup>10</sup> However, for rougher and less correlated surfaces such as the liquid metal considered here, it is expected to have smaller values reflecting the smaller range of correlation for the surface vibrations. A table of values of  $v_R$  obtained for a number of different surfaces and atomic projectiles is given in Ref. 13.

Another model, which has also been used to discuss rare-gas scattering from surfaces, regards the surface as a collection of discrete scattering centers. In this case, the correlation between different scattering centers is lost and the parameter  $v_R=0$ . However, the correct classical differential reflection coefficient is not obtained from Eq. (1) simply by taking the limit  $v_R \rightarrow 0$ . The correct derivation for this model produces an expression which differs from Eq. (1) not only in that the Gaussian-like term in parallel momentum transfer disappears, but also the prefactor involving  $\Delta E_0$  and  $T_S$  appears raised to the power  $\frac{1}{2}$  instead of  $\frac{3}{2}$ . The differential reflection coefficient for this discrete model is given by

$$\frac{dR(\mathbf{p}_f, \mathbf{p}_i)}{d\Omega_f dE_f} = \frac{m^2 |\mathbf{p}_f|}{8\pi^3 \hbar^4 p_{iz}} |\tau_{fi}|^2 \left( \frac{\pi}{\Delta E_0 k_B T_S} \right)^{1/2} \times \exp \left\{ - \frac{(E_f - E_i + \Delta E_0)^2}{4k_B T_S \Delta E_0} \right\}. \quad (2)$$

Equation (1) has been shown to give the correct temperature and energy dependence for He atom scattering from metal surfaces in the classical limit of high incident energies and large surface temperatures.<sup>13,14</sup> For ion scattering at much higher energies the discrete model of Eq. (2) appears to apply,<sup>15</sup> and this is reasonable because high-energy ions would be expected to interact with the hard cores of the substrate atoms and not with the much weaker electron density extending outside the surface layer which is the origin of the repulsive force experienced by low-energy atomic projectiles.

The final quantity needed in order to fully specify the differential reflection coefficient of Eq. (1) is the form factor  $|\tau_{fi}|^2$ . A constant form factor is correct for classical hard-sphere scattering, however, this is not appropriate for scattering from a smooth repulsive barrier. Instead, the semiclassical form factor can be obtained from the quantum-mechanical transition matrix in the appropriate limit. The quantum-mechanical form factor is given by the transition matrix of the elastic part of the interaction potential extended off the energy shell to final momenta corresponding to the inelastic translational energy loss.<sup>16</sup> For example, a widely utilized form factor for elastic and inelastic He atom scattering is the Jackson-Mott form which is the matrix element of an exponentially repulsive potential, e.g.,  $V(z) = V_0 \exp(-\beta z)$ , taken with respect to its own eigen-

functions.<sup>17</sup> In the semiclassical limit of a hard, repulsive barrier  $\beta \rightarrow \infty$  this (and all other similar matrix elements) go to the limit<sup>18</sup>

$$\tau_{fi} = 4p_{fz}p_{iz}/m. \quad (3)$$

The differential reflection coefficient of Eq. (1) combined with the form factor of Eq. (3) constitute a smooth, flat surface, classical model for the scattering which depends on only the single parameter  $v_R$  and this is the primary model used here to compare with experiment.

However, there are other more elaborate forms that classical models can take. An intermediate model, which connects the discrete model of Eq. (2) and the flat surface model of Eq. (1), has been obtained by considering a smooth but corrugated potential barrier.<sup>7</sup> By using models based on the form of the scattering source function for a hard wall corrugated surface, this intermediate classical model produces a differential reflection coefficient of the form

$$\frac{dR(\mathbf{p}_f, \mathbf{p}_i)}{d\Omega_f dE_f} = \frac{m^2 |\mathbf{p}_f|}{8\pi^3 \hbar^4 p_{iz}} |\tau_{fi}|^2 \left( \frac{\pi}{\Delta E_0 k_B T_S} \right)^{1/2} \times \exp \left\{ - \frac{(E_f - E_i + \Delta E_0)^2}{4k_B T_S \Delta E_0} \right\} \times \left[ \frac{\gamma^2}{k_B T_S \Delta E_0 / 2 \hbar^2 v_R^2 + \gamma^2} \right] \times \exp \left\{ - \frac{\mathbf{P}^2}{4(k_B T_S \Delta E_0 / 2 v_R^2 + \hbar^2 \gamma^2)} \right\}, \quad (4)$$

where  $\gamma$  is the corrugation parameter of the source function. In the limit of small  $\gamma$  (nearly flat surface) Eq. (4) reduces to the continuum model of Eq. (1), while in the limit of large  $\gamma$  it goes to the limit of Eq. (2). For the scattering of Ar from liquid In and Ga, the temperature dependence of the energy-resolved scattering data has been explained by the intermediate model of Eq. (4) with a value for the parameter  $\gamma = 20 \text{ \AA}^{-1}$  and  $v_R = 400 \text{ m/s}$ .<sup>7</sup>

### III. RESULTS

Figure 1 shows experimental data points for a series of three polar plots exhibiting the scattered total angular intensities for three different incident energy monoenergetic beams of Ar incident at an angle of  $55^\circ$  with respect to the surface normal on a liquid In surface at a temperature of 436 K (6 K above the melting temperature). One is immediately struck by the fact that this data clearly shows behavior which is far from an equilibrium distribution, as a gas in equilibrium with the surface would have the Knudsen cosine distribution which appears in a polar plot as a circle tangent to the origin. The lobes shown as solid curves in Fig. 1 are calculated from Eq. (1) with the form factor of Eq. (3). The theoretical curve plotted is  $dR/d\Omega_f$ , which is the integral of Eq. (1) over all final energies.

Quite good agreement with the data is achieved with a value of  $v_R \approx 450 \text{ m/s}$  at the incident energies  $E_i = 36$  and  $96 \text{ kJ/mole}$  (373 and 995 meV). At the lowest incident energy of  $6 \text{ kJ/mole}$  (62 meV) a smaller value of  $v_R = 100 \text{ m/s}$  was used. In solids the value of  $v_R$  is expected to be smaller than

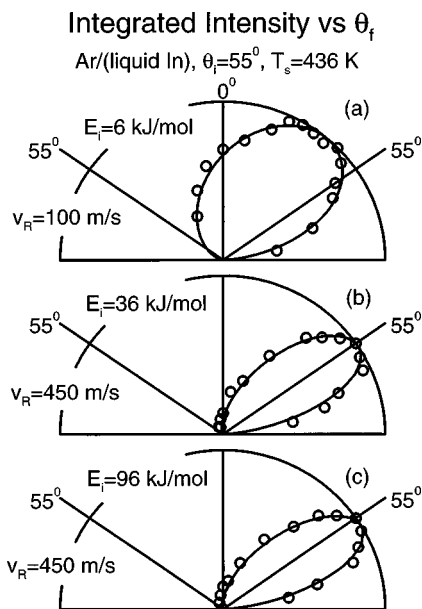


FIG. 1. Polar plots of angular lobes for Ar scattered by liquid In at  $T_s = 436$  K for the three incident energies  $E_i = 6, 36,$  and  $96$  kJ/mole as marked. The incident angle is  $55^\circ$ . The solid curves are the theoretical calculations with the corresponding values of  $v_R$  indicated.

the bulk or surface wave velocity (the sound velocity in liquid Ar is  $2215$  m/s at its melting temperature<sup>19</sup>), and for liquids where the correlation between atoms is less than in solids  $v_R$  is expected to be even smaller. Thus the values of  $v_R$  obtained here are well within expectations.

It is argued below in connection with Fig. 4 that the smaller value of  $v_R$  required for the lowest incident energy using the simple flat repulsive barrier model of Eq. (1) is primarily due to neglect of the attractive van der Waals adsorption potential. The depth of this potential well is probably similar to that expected for typical metal surfaces where for Ar it has been variously estimated at roughly  $40$ – $100$  meV,<sup>1,20</sup> thus the well depth may be comparable to the incident energy in this case.

It is of interest to note that for the angular distribution lobes of Fig. 1, good agreement is found with the continuum model of Eq. (1), but not with the discrete model of Eq. (2). The discrete model produces lobes which are too broad and whose most probable intensities are not at the correct positions, regardless of which of the two form factors are used, a constant or the hard wall expression of Eq. (3). In principle, of the two form factors, only the constant form factor is appropriate for the discrete model on physical grounds, and this gives quite poor agreement with the angular distributions. At first glance this result seems to be in disagreement with the fact that in earlier work the energy-resolved time-of-flight (TOF) intensity distributions for this same Ar–In system were explained rather well using the discrete model, with the inclusion of multiple scattering with the surface atoms.<sup>15</sup> The explanation for this apparent contradiction is that both the discrete and continuum models produce very similar results for the energy-resolved intensities if one limits the comparison to scattered angles near to the maximum (or most probable) intensities and for a single surface tem-

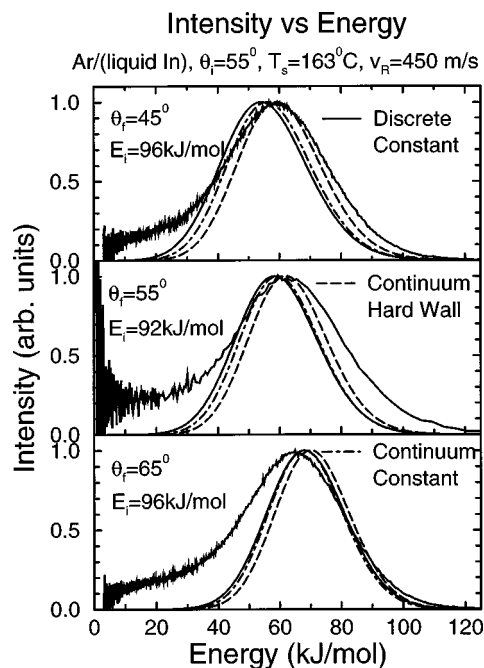


FIG. 2. Comparison of three different classical models with the experimental data at  $96$  and  $92$  meV and for the three incident angles of  $\theta_i = 45^\circ, 55^\circ,$  and  $65^\circ$ . The calculations are for single scattering only, in which the solid curve is the discrete model of Eq. (2) with a constant form factor, the dashed curve is the continuum model of Eq. (1) with the hard wall form factor of Eq. (3), and the dash-dot curve is the continuum model with a constant form factor. Each panel contains calculations using all three of these models. The discrete model contains no parameters, while for both of the continuum model curves  $v_R = 450$  m/s.

perature. Such a comparison is shown in Fig. 2 which compares the TOF data (converted to energy transfer) at an incident energy  $E_i \approx 1$  eV at three angles near the most probable intensity of about  $\theta_f = 50^\circ$  with both the discrete and continuum models. The three calculated curves are for the discrete model with a constant form factor, and two curves for the continuum model using  $v_R = 450$  m/s, one with the constant form factor and one with the hard wall form factor. Only the single scattering contribution is shown in each case. It is immediately apparent that all of these calculated curves are quite similar in shape and are distinguished only by a slight difference in the position of the maximum. Only if the correlation parameter  $v_R$  is raised to values larger than  $500$  m/s does the continuum model produce an intensity peak appreciably narrower than the discrete model.

Thus, on the sole basis of TOF data taken at angles near to the maximum intensities (which in this case is also near to the specular direction) it appears difficult to distinguish between the discrete and continuum models. Of course, the two models do have a different dependence on surface temperature which is clear from the envelope factors of Eqs. (1) and (2), and we discuss this aspect further below in connection with Fig. 5.

It is also of importance to note from Fig. 2 that the single scattering contribution alone does a moderately reasonable job of matching the width and shape of the measured energy-resolved intensities and appears to dominate the area under the intensity curve. In the earlier work it was found that the multiple scattering contributions were important in matching

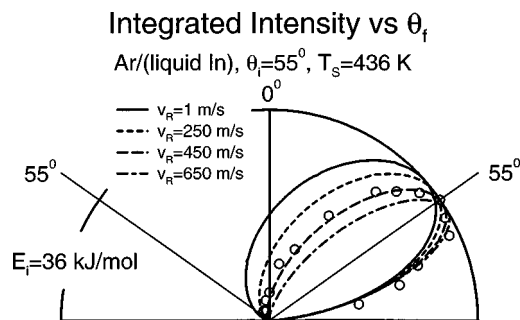


FIG. 3. Calculated dependence on  $v_R$  of the angular distribution lobe of Ar scattering from liquid In with  $E_i = 36$  kJ/mole (373 meV) as in Fig. 1. The parameter  $v_R$  takes on the values  $v_R = 1, 250, 450,$  and  $650$  m/s as marked.

the calculations to the high- and low-energy tails of the data,<sup>15</sup> while the single scattering term was the dominant contribution to the total intensity.

Figure 3 shows calculated predictions at the incident beam energy of 36 kJ/mole (373 meV) for the dependence of the angular distributions on the parameter  $v_R$ . Figure 3 shows that the effect of increasing the value of  $v_R$  is to narrow the scattered angular distribution lobe and to shift its center away from the normal direction (supraspecular shift). This is to be expected because, as seen from the Gaussian-like term in the parallel momentum transfer in Eq. (1), the effect of a large  $v_R$  is to restrict the final parallel momentum to values very close to the incident parallel momentum. However, the dependence on  $v_R$  is not strong, and reasonable agreement with the data is still obtained if  $v_R$  is varied by as much as 10% about its optimal value.

Up to this point the scattering data has been treated with a theory based on a purely repulsive interaction potential. However, the van der Waals force between the surface and the incident atomic projectile creates an attractive well in front of the surface. In the case of purely classical scattering the primary effect of the van der Waals attractive potential is to accelerate the incoming particle in the direction normal to the surface. This is a refractive effect quite similar to the familiar Snell's law of optics in refractive media. Since refraction is the dominant effect, the potential can be modeled by a one-dimensional potential well and for a given well depth  $D$  the refraction does not depend on the shape of the attractive part. Thus, this attractive force can be modeled by an attractive one-dimensional square-well potential in front of the repulsive barrier. If the well is made wider than the selvedge region of the surface, where the selvedge region is bounded by the maximum and minimum extents of the corrugation of the hard repulsive wall, then its width is unimportant, and the effect on the collision process is to replace the perpendicular component of the momentum  $p_{qz}$  near the surface by an enhanced value  $\tilde{p}_{qz}$  which includes the well depth  $D$

$$\tilde{p}_{qz}^2 = p_{qz}^2 + 2mD. \quad (5)$$

This model of the attractive potential refracts all projectiles at the leading edge of the well and causes them to collide with the barrier with a higher normal energy. The effects of the attractive potential well on the scattering are displayed in

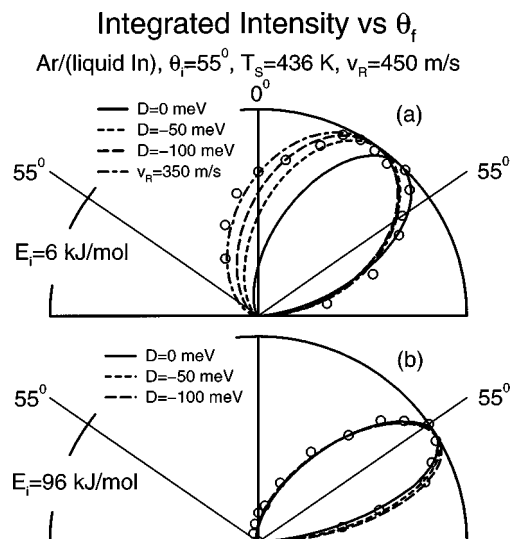


FIG. 4. Dependence of the scattered angular distribution on the depth of the attractive potential well for the scattering of Ar from liquid In at  $T_S = 436$  K. (a)  $E_i = 6$  kJ/mol, and (b)  $E_i = 96$  kJ/mol as in Fig. 1. The three calculated curves are for well depths of  $D = 0$  (solid curve),  $D = 50$  meV (short-dashed curve), and  $D = 100$  meV (long-dashed curve), all with the parameter  $v_R = 450$  m/s. Additionally, on graph (a) for  $E_i = 6$  kJ/mol the dash-dot curve shows a somewhat better fit with  $D = 100$  meV and  $v_R = 350$  m/s.

Fig. 4 for the smallest and largest incident energies,  $E_i = 6$  and 96 kJ/mol, shown in Fig. 1. The angular distribution data are compared to the continuum model calculation with well depths of  $D = 0, 50,$  and  $100$  meV (0, 4.8, and 9.6 kJ/mol; the solid, dashed, and long-dashed curves, respectively), all with the same  $v_R = 450$  m/s value used for the two higher energy angular distributions in Fig. 1. Clearly the effect of the potential well is to give a considerable broadening to the calculated angular distribution. The calculation with a rather large well of depth  $D = 100$  meV is not far from being in reasonable agreement with the data, and if  $v_R$  is reduced to 350 m/s (dash-dot curve) the agreement is rather good, as is also shown in the top panel of Fig. 4. The bottom panel of Fig. 4 shows similar calculations compared with the experimental lobe data for the highest energy of  $E_i = 96$  kJ/mol and here it is seen that the well, which in this case is much smaller than the incident energy, has little effect on the results. Thus, it appears that the van der Waals attractive potential well can explain much of the reason why a smaller value of  $v_R$  was needed at low energy in order to match the angular distribution data with a simple repulsive barrier.

The temperature dependence of the angular distributions are shown in Fig. 5 for the two different incident energies  $E_i = 6$  and 96 kJ/mol and two surface temperatures,  $T_S = 436$  and 586 K. Also shown in each panel of Fig. 5 are two calculated curves for  $T_S = 436$  and 586 K as explained in more detail below. In the experimental measurements taken at the higher energy there is a noticeably strong  $T_S$  dependence, however, this is much less apparent at the lower energy where in fact at some angles the experimental error bars are overlapping for the points taken at the two different temperatures.<sup>6</sup> As  $T_S$  is increased the angular distribution lobe broadens, and its most probable intensity decreases and

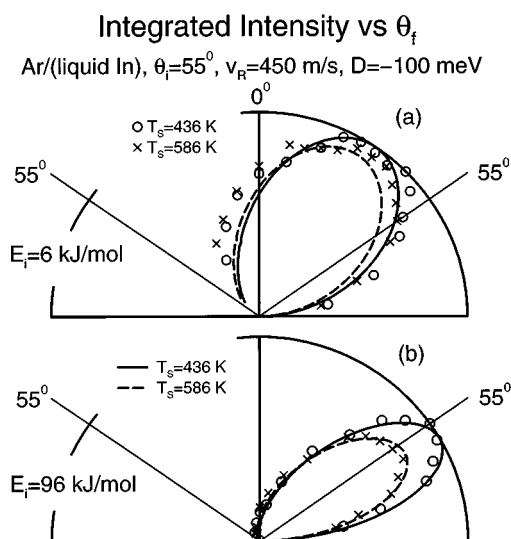


FIG. 5. Dependence of the scattered angular distribution on surface temperature for Ar scattering from liquid In at the two incident energies (a)  $E_i = 6$  kJ/mol, and (b)  $E_i = 96$  kJ/mol. On each polar plot are shown the experimental data for the two temperatures  $T_S = 436$  K (open circles, same as in Fig. 1) and 586 K ( $\times$ ). The calculations are as follows: for  $E_i = 6$  kJ/mol the solid curve is the continuum model with  $D = 100$  meV and  $v_R = 450$  m/s as in Fig. 4 and for  $E_i = 96$  kJ/mol the solid curve is the continuum model with  $D = 0$  and  $v_R = 450$  m/s, both for  $T_S = 436$  K. The dashed curves are the same calculations with  $T_S = 586$  K.

shifts toward the surface normal (subspecular shift). The broadening of the lobe is due to the larger range of final states available to a scattered particle at higher temperatures, and concomitant with the broadening, the magnitude of the most probable intensity must decrease as is required by the unitarity of the ratio of numbers of incident to outgoing scattered particles. The shift towards the subspecular direction is expected because the average energy of the scattered particles increases with the surface temperature.

The calculations shown at high incident energy in Fig. 5(b) are for the simplest continuum model without a potential well. The broadening, shift, and absolute decrease in maximum intensity observed in the data at the higher temperature of  $T_S = 586$  K are correctly predicted by the continuum model calculation as seen in Fig. 5(b). If a well is included in the calculation the results change very little, as indicated previously in connection with Fig. 4.

The calculations shown in Fig. 5(a) for the smaller incident energy are done with the parameters from Fig. 4(a) ( $v_R = 450$  m/s and a well depth  $D = 100$  meV). In this case, the broadening, subspecular shift, and the decrease in maximum intensity are much less pronounced than for the higher energy case of Fig. 5(b). Again, the calculations match the small temperature-dependent changes in the data reasonably well. The presence of the attractive potential well is not expected to have an appreciable effect on the temperature dependence of the calculations, and in order to check this calculation were also carried out for the parameters of Fig. 1(a) ( $v_R = 100$  m/s and  $D = 0$ ) as well as for the better-fit parameters of Fig. 4(a) ( $v_R = 350$  m/s and  $D = 100$  meV) and in all cases the agreement with the experimental data is very similar to that of Fig. 5(a).

It is interesting that the temperature-dependent change in the shape and intensity of the scattered lobe at low incident energy is much smaller than for the higher incident energy. The primary reason for this is that at the lower energy the average energy of an incident Ar atom is smaller than the average vibrational kinetic energy of a surface atom. Thus the average fractional energy loss of the incident beam is significantly less when making a single collision than is the case for incident energies which are much higher than that of a typical surface atom. It should also be noted that at the lower incident energy of 6 kJ/mol it is difficult to exclude the possibility of a contribution to the scattered intensity due to trapping in the adsorption well with subsequent thermal diffuse emission.<sup>21</sup> Previous energy-resolved TOF measurements at incident energies higher than 6 kJ/mol have demonstrated that there is no significant diffuse signal for those larger energies,<sup>4,5</sup> but for the combination of surface temperatures and the low incident energy used here, it is difficult to distinguish the direct scattered and thermal diffuse signals in a TOF experiment. Thus despite the reasonable agreement shown in Fig. 5, a small contribution due to thermal diffuse emission cannot be ruled out.

The theoretical temperature dependent behavior found here for the angular distributions is somewhat surprising when compared to the temperature dependence found for the energy-resolved data.<sup>5</sup> As was demonstrated in Ref. 4, at a given temperature the discrete model predicts rather well the forms of the TOF intensities as a function of final energy, as does also the continuum model as shown in Fig. 2. However, the decrease of the most probable intensity with increasing  $T_S$  was not correctly given by either of these models, the  $T_S^{-3/2}$  dependence predicted by the continuum model of Eq. (1) being too rapid, and the  $T_S^{-1/2}$  behavior of the discrete model of Eq. (2) being not rapid enough. The intermediate model (4), however, with parameters  $v_R = 400$  m/s and  $\gamma = 20 \text{ \AA}^{-1}$  gave good agreement with the available TOF data for both Ar-In and Ar-Ga, thus the temperature dependence of the energy-resolved TOF data would indicate that the liquid metal surface is corrugated as expected. However, the temperature-dependent data for the angular distribution lobes considered here (albeit, currently limited to only two temperatures) are consistent with the predictions of the simpler continuum model.

It is of interest to use the continuum model to make further predictions of the temperature-dependent characteristics of the angular distributions. The subspecular shift of the most probable intensity with increasing temperature is rather substantial and amounts to about  $10^\circ$  between the melting point of In and  $T_S = 1000$  K. The decrease of the most probable intensity of the calculated angular distribution lobes is rather strong, and follows approximately a  $T_S^{-3/4}$  dependence. The full width at half maximum (FWHM) of the lobe increases with  $T_S$  approximately with the power law  $T_S^{1/3}$  under the conditions of Fig. 5. It is interesting to note that the temperature dependence as a function of final angles of the FWHM for the angular distribution lobe is, as expected, less strong than the FWHM as a function of energy of the TOF energy-resolved peaks, which for all the classical models increases very nearly as  $T_S^{1/2}$ .

#### IV. CONCLUSIONS

One of the conclusions that one can draw from the agreement shown in Fig. 1 is that the primary shape of the scattered lobes is determined by single scattering events. This conclusion is consistent with the fact that the lobes show distinctly nonequilibrium behavior. In order to achieve equilibrium, incoming particles would have to make many collisions with the surface in order to attain a Maxwell–Boltzmann distribution, which is clearly not the case here. At first glance this conclusion about the predominance of single scattering would appear to be in contradiction to earlier theoretical comparisons with the energy-resolved data for these same systems, where it was found that additional multiple scattering was necessary in order to fully agree with the measured TOF data.<sup>4</sup> However, in this previous work the single scattering contribution was dominant, and the multiple scattering was needed mainly to obtain agreement with the observed intensity in the low- and high-energy tails of the distribution. Thus these measurements of total angular distributions, which at each final angle consist of the integral over all final energies, also appear to be dominated by the single scattering contribution.

An equally important conclusion is that the range of classical scattering models which can explain the measurements is rather severely restricted by these new experiments. The model which agrees with the current angular distribution data taken at temperatures  $T_S=436$  and 586 K is the continuum model of Eq. (1) for a smooth repulsive barrier taken together with the semiclassical hard wall form factor of Eq. (3), and at low incident energy the adsorption well must be included in the potential. Similar calculations carried out with the discrete particle model, which was previously used to analyze the earlier energy-resolved TOF data for this same Ar–In system,<sup>4</sup> do not agree with the observed lobes. The single parameter  $v_R$  contained in the smooth barrier model takes on values which are well within the expected range. Furthermore, this velocity has an important physical meaning, it is a measure of the correlation between nearby points on the surface, and can in principle be calculated independently of the scattering process.<sup>10,11</sup>

Clearly, a smooth, flat repulsive barrier as embodied in the form factor of Eq. (3) is an overly simplistic view of the molten metal surface, which must in reality be somewhat rough. In fact, the importance of the surface roughness is evident in the fact that the earlier analysis of the TOF data required a corrugated surface in order to obtain agreement with the temperature dependence.<sup>7</sup> However, the success of the simple flat-surface model for the form factor utilized here can be understood by examining its theoretical origins. The form factor can be identified from the full quantum version of multiphonon theory as the transition matrix of the elastic part of the interaction potential evaluated off the elastic energy shell.<sup>12,16</sup> The Jackson–Mott matrix element of Eq. (3) is exactly this transition matrix element, evaluated in the distorted wave Born approximation and for a flat hard wall barrier. The logical way to treat the problem of a corrugated surface is to expand the elastic interaction potential in a Fourier series. The quasi-periodicity of the liquid surface will produce higher order Fourier components, and the zero order

Fourier component will describe a flat surface potential (the average surface) and the limiting hard wall form for its semiclassical matrix elements will be identical with that of Eq. (3). Thus, if the surface is not too rough, implying that the higher order Fourier components are not large, then the current continuum model can still give a good description of the integrated angular lobes considered here. However, even in the case in which the higher order Fourier components are not small, implying a rough surface, the  $z$ -dependence of the repulsive part of all Fourier components of the potential will be approximately exponential in form. Since the Jackson–Mott matrix element is the matrix element of an exponentially repulsive potential, all Fourier components would be multiplied by the Jackson–Mott matrix element, which in the hard wall barrier limit becomes Eq. (3). The above argument implies that the form factor of even a rough surface, in the hard wall limit, will contain as an approximate multiplicative factor, the Jackson–Mott function of Eq. (3).

Not surprisingly, it is found that the adsorption potential well in front of the surface barrier plays a large role in shaping the scattered angular distribution when the incident energy is small. Although the simple square-well model adopted here does not have the correct  $1/z^3$  behavior of the leading term of the attractive van der Waals potential, it does correctly produce the refraction effects and the higher energy of collision into the repulsive barrier due to the well. The refraction and higher normal energy of collision are the major effects of an attractive well in classical scattering, since the backscattering of incoming projectiles by the attractive van der Waals force will be negligible. The main effect of the inclusion of an attractive well, as compared to a potential with no well, is to broaden the scattered angular distribution lobes when the incident energy is comparable to or not too much larger than the well depth.

The present theoretical analysis of the data currently available for the scattering of Ar from liquid In surfaces has produced a clearer picture of the scattering process. The shape of the energy-resolved scattered intensities is rather well explained with a classical model in which single scattering events are dominant, but multiple scattering is necessary in order to describe the high- and low-energy tails of the energy distribution.<sup>4</sup> As shown in Fig. 2, either the discrete or continuum surface models of Eqs. (1) or (2) is adequate to describe the energy-resolved TOF data taken at a single temperature and at final angles near to the maximum in the angular distributions. The newly available data for the total scattered angular lobes analyzed here are explained with a smooth-barrier classical single scattering model with the additional features of an attractive well and a hard wall form factor. In fact, the good agreement obtained with the angular distribution data using the continuum model, and the inability to match the same data with the discrete model, appears to exclude the discrete surface model.

The model used here is quite similar to potential models which have been successful in describing He atom scattering from crystal metal surfaces,<sup>1,3</sup> where the potential has a

smooth but corrugated repulsive barrier. This repulsive barrier is due to the Pauli exchange forces arising from the overlap of the He atomic electrons and the decaying electronic density in front of the metal surface. He atom cattering from insulator surfaces, for example, alkali halides, is also characterized by a continuous corrugated repulsive barrier but analysis of multiphonon scattering experiments shows that the values of  $v_R$  obtained for such insulator surfaces are significantly higher than those obtained for metals.<sup>22</sup> The similarity of the present models to the He scattering potentials, in particular the use of the smooth-surface model with a relatively small value of  $v_R$ , indicates that the In surface is still metallic in nature even in the liquid state.

The fact that this newly available data on the scattering lobes of the Ar-In liquid system leads to further restrictions on the scattering models and a better understanding of the scattering process clearly points out the need for more experiments on both the energy-resolved and angular distributions for a larger range of initial conditions, i.e., incident angles, energies, and surface temperatures. This work would suggest that more data on the temperature dependence of both the angular distribution lobes and the energy-resolved spectra would be extremely helpful in determining the nature and extent of the surface corrugation. Future theoretical work on this and related rare gas scattering systems will surely need to take into account more sophisticated models for the interaction potential between the incoming projectiles and the surface, and classical molecular-dynamics simulations are probably the method of choice.<sup>9,23</sup> However, the relatively straightforward scattering models used here agree quite well with the available experimental data and have the additional benefit of producing analytical solutions, such as Eqs. (1) and (2), which are extremely useful for predicting the physical responses of systems over a wide range of initial conditions. Furthermore, the success of these models in explaining the experimental results demonstrates the complete validity of using classical dynamics for more detailed numerical simulations of this system.

## ACKNOWLEDGMENTS

The authors would like to thank G. Nathanson, M. Manning, and J. Morgan for helpful discussions and for permission to use their data prior to publication. This work was supported by the NSF under Grant No. DMR 9726229 and by the DOE under Grant No. DE-FG02-98ER45704.

- <sup>1</sup>H. Hoinkes, *Rev. Mod. Phys.* **52**, 933 (1980).
- <sup>2</sup>V. Bortolani and A. C. Levi, *Rivista del Nuovo Cimento* **9**, 1 (1986).
- <sup>3</sup>*Helium Atom Scattering from Surfaces*, edited by E. Hulpke, of the Springer Series in Surface Science (Springer, Heidelberg, 1992), Vol. 27.
- <sup>4</sup>A. Muis and J. R. Manson, *J. Chem. Phys.* **107**, 1655 (1997).
- <sup>5</sup>W. R. Ronk, D. V. Kowalski, M. Manning, and G. M. Nathanson, *J. Chem. Phys.* **104**, 4842 (1996).
- <sup>6</sup>M. Manning, J. A. Morgan, and G. M. Nathanson, *J. Chem. Phys.* (to be submitted).
- <sup>7</sup>J. R. Manson, *Phys. Rev. B* **58**, 2253 (1998).
- <sup>8</sup>V. Celli, in Ref. 3, p. 25.
- <sup>9</sup>L. Tribe, M. Manning, J. A. Morgan, M. D. Stephens, W. R. Ronk, E. Treptow, G. M. Nathanson, and J. L. Skinner, *J. Phys. Chem.* **102**, 206 (1998).
- <sup>10</sup>R. Brako and D. M. Newns, *Phys. Rev. Lett.* **48**, 1859 (1982); *Surf. Sci.* **123**, 439 (1982).
- <sup>11</sup>H.-D. Meyer and R. D. Levine, *Chem. Phys.* **85**, 189 (1984).
- <sup>12</sup>J. R. Manson, *Phys. Rev. B* **43**, 6924 (1991).
- <sup>13</sup>F. Hofmann, J. P. Toennies, and J. R. Manson, *J. Chem. Phys.* **106**, 1234 (1997).
- <sup>14</sup>M. Bertino and J. R. Manson, *J. Chem. Phys.* **108**, 10239 (1998).
- <sup>15</sup>A. Muis and J. R. Manson, *Phys. Rev. B* **54**, 2205 (1996).
- <sup>16</sup>J. R. Manson, *Comput. Phys. Commun.* **80**, 145 (1994).
- <sup>17</sup>J. M. Jackson and N. F. Mott, *Proc. R. Soc. London, Ser. A* **137**, 703 (1932).
- <sup>18</sup>F. O. Goodman and H. Y. Wachman, *Dynamics of Gas-Surface Scattering* (Academic, New York, 1976).
- <sup>19</sup>W. Schaafs, in *Landolt-Börnstein, Group II, Vol. 5* (Springer-Verlag, Heidelberg, 1967).
- <sup>20</sup>E. K. Schweitzer, C. T. Rettner, and S. Holloway, *Surf. Sci.* **249**, 335 (1991).
- <sup>21</sup>G. Nathanson, private discussion.
- <sup>22</sup>G. G. Bishop, E. S. Gillman, Jeff Baker, J. J. Hernaández, S. A. Safron, J. G. Skofronick, S. M. Weera, and J. R. Manson, *Phys. Rev. B* **52**, 13229 (1995); **52**, 14185 (1995).
- <sup>23</sup>B. Gerber *et al.*, (to be published).